One of the present authors (KY) expresses his sincere thanks to Professor J. M. Cowley for providing him with the opportunity to stay at ASU and for his continuous encouragement. Thanks are also due to Dr S. Iijima for much technical advice and discussion concerning high-resolution electron microscopy. This work was partially supported by the Ministry of Education of Japan and by USA National Science Foundation grants GH 36668 and DMR 76-06108.

References

COWLEY, J. M. & IIJIMA, S. (1973). *Z. Naturforsch. Teil A*, **27**, 445–451.

FALLON, G. D. & GATEHOUSE, B. M. (1977). *J. Solid State Chem.* **22**, 405–409.

GATEHOUSE, B. M. (1976). *J. Less-Common Met.* **50**, 139–144.

GROULT, D., CHAILLEUX, J. M., CHOISNET, J. & RAVEAU, B. (1976). *J. Solid State Chem.* **19**, 235–244.

IIJIMA, S. (1971). *J. Appl. Phys.* **42**, 5891–5893.

MINOR, D. B., ROTH, R. S., PARKER, H. S. & BROWER, W. S. (1977). *J. Res. Natl Bur. Stand.* **82**, 151–165.

ROTH, R. S., BROWER, W. S., PARKER, H. S., MINOR, D. B. & WARING, J. L. (1975). *NASA Contract. Rep.* CR-134869.

YAGI, K. & ROTH, R. S. (1978). *Acta Cryst.* A**34**, 773–781.

Acta Cryst. (1978). A**34**, 773–781

Electron-Microscope Study of Crystal Structures of Mixed Oxides in the Systems Rb_2O–Ta_2O_5, Rb_2O–Nb_2O_5 and K_2O–Ta_2O_5 with Composition Ratios Near 1:3. II. Various Intergrowth Phases and Two-Dimensional Ordering of Pentavalent Ions

BY K. YAGI*

Physics Department, Arizona State University, Tempe, AZ 85281, *USA*

AND R. S. ROTH

National Bureau of Standards, Washington, DC 20234, *USA*

(*Received* 13 *January* 1978; *accepted* 15 *March* 1978)

In part I, the preceding paper, structural models were proposed on the basis of high-resolution electron microscopy for phases previously designated as 11*L*, 9*L* and 16*L*, which were found to exist in the title systems. Two types of blocks were found, which are composed of five and six layers of octahedra. In the present paper, various intergrowth phases which are composed of the two types of blocks are described. A new notation is proposed to denote these intergrowth phases as well as the 11*L*, 9*L* and 16*L* structures. Two-dimensional ordering of pentavalent ions in the six-layer block is found, giving rise to diffuse scattering in electron diffraction patterns. Two-dimensional images, calculated on the basis of the proposed model, are found to reproduce the observed images.

1. Introduction

In part I (Yagi & Roth, 1978) structure models were proposed from the high-resolution structure images taken in a modified high-resolution microscope (Iijima, 1971) for the 11*L*, 9*L* and 16*L* structures which were found to exist commonly in the mixed oxides Rb_2O–Nb_2O_5, Rb_2O–Ta_2O_5 and K_2O–Ta_2O_5. The structures are closely related to the pyrochlore structure and are summarized in Table 1. In the pyrochlore structure, hexagonal tungsten bronze (HTB) like octahedron layers and isolated-octahedron layers are alternately stacked in the way *AaBbCc*.... Two types of blocks, which are composed of five and six octahedron layers,

Table 1. *Summary of structures*

Structures	Stacking sequences
Pyrochlore structure (mirror structure)	*AaBbCcAa*... *A'c'C'b'B'a'A'c'*...
11*L* structure (1-0 *R*) (mirror structure)	ABCABC... A'C'B'A'C'B'...
9*L* structure (0-1 *H*)	$B_0A'_0B_0A'_0$...
16*L* structure (1-1 *H*)	$BC_0B'A'_0BC_0B'$...
Sequence rules of blocks	AB, AB_0 (cyclic) A'C', $A'C'_0$ (cyclic) A_0C', $A_0C'_0$ (cyclic) A'_0B, A'_0B_0 (cyclic)
A : *CcAaB* (cyclic) A_0: *CcAA'c'C'* (cyclic)	A': *B'a'A'c'C'* (cyclic) A'_0: *B'a'A'AaB* (cyclic)

* Present address: Physics Department, Tokyo Institute of Technology, Oh-okayama, Meguro-ku, Tokyo 152, Japan.

were found in these mixed oxides. They are denoted A,B,C,A′,B′,C′ and A_0,B_0,C_0,A'_0,B'_0,C'_0, respectively, depending on the types of octahedron layers forming the structure. With this notation, the 11*L*, 9*L* and 16*L* structures can be written as in Table 1. As discussed in part I, octahedra in the HTB-like layers, which connect neighboring blocks, are tilted to some extent, so that there are sequence rules for these blocks, as shown in Table 1.

In the present paper, part II, various intergrowth phases are described which are composed of the two types of blocks with the block-sequence rules in Table 1. A new notation is proposed to describe these phases as well as the 11*L*, 9*L* and 16*L* structures. A two-dimensional ordering of pentavalent ions in the six-layer block is observed. The observed images are compared with those calculated based upon the proposed structure model.

2. Results

2.1. *Intergrowth phases*

(*a*) *Notations for the various phases.* All observed phases can be described by *n-m H* or *n-m R*, where *n* and *m* are numbers of successive blocks of the five and six-layer blocks, respectively, *i.e.* unit cells are composed of *n* five-layer blocks and *m* six-layer blocks. *H* and *R* are used to describe the hexagonal *ABAB* and rhombohedral *ABCABC* arrangements of the unit composed of $(n + m)$ blocks. An important fact, which is a direct consequence of the block-sequence rules, is that *R* and *H* correspond to the cases of $m = 0$ or even and $m =$ odd respectively.

With this notation it is evident from Table 1 that the 11*L* and 9*L* structures can be written as 1-0 *R* and 0-1 *H* respectively. In the former case the unit is composed of one five-layer block and three units correspond to the *c* lattice period; in the latter case, two units correspond to the *c* lattice period. The 16*L* structure is 1-1 *H*, where two units, each of which is composed of (1 + 1) blocks, form the unit cell. For the case $n = 2$, $m = 1$, the sequence of blocks can be written as follows, following the sequence rules and starting from the A type block, $ABC_0B'A'C_0ABC_0\ldots$, and the phase can be written as 2-1 $H(m =$ odd). For $n = 1$, $m = 2$, the block sequence would be $AB_0A'_0BC_0$-$B'_0CA_0C'_0A\ldots$ and can be written as 1-2 $R(m =$ even).

(*b*) *Observed intergrowth phases.* The observed phases are summarized in Table 2 and some of them are shown in Figs. 1–4. Fig. 1 shows an electron micrograph of the 1-2 *R* structure. Small and large arrows indicate the positions of the five and six-layer blocks respectively. In this case the incident beam is not exactly parallel to the $[010]_h$ axis, so the white-spot arrangement is not clearly seen in the thicker area. However, in Fig. 1 all the five-layer blocks are of similar character, *A*,*B*,*C* or *A*′,*B*′,*C*′. The hole sequence is seen to be *ab-bb-bb-bc-cc-cc-ca* . . .. Thus the structure can be written as 1-2 *R*.

Fig. 2 shows a crystallite which contains a small region of 2-1 *H* structure. The micrograph is taken under the condition of $[\bar{1}10]_h$ incidence. From this direction the hole sequence is not seen. The positions of the five and six-layer blocks are indicated by small and

Table 2. *Observed phases*

1-0 *R* (11*L*)	ABCABC...
0-1 *H* (9*L*)	$A_0C'_0A_0C'_0$...
1-1 *H* (16*L*)	$AB_0A'C'_0AB_0$...
1-2 *R*	$AB_0A'_0BC_0B'_0CA'_0A$...
2-1 *H*	$ABC_0B'A'C'_0A$...
1-4 *R*	$A(B_0A'_0)\times 2$ $B(C_0B'_0)\times 2$ $C(A_0C'_0)\times 2$ A...
1-8 *R*	$A(B_0A'_0)\times 4$ $B(C_0B'_0)\times 4$ $C(A_0C'_0)\times 4$ A...
1-14 *R*	$A(B_0A'_0)\times 7$ $B(C_0B'_0)\times 7$ $C(A_0C'_0)\times 7$ A...

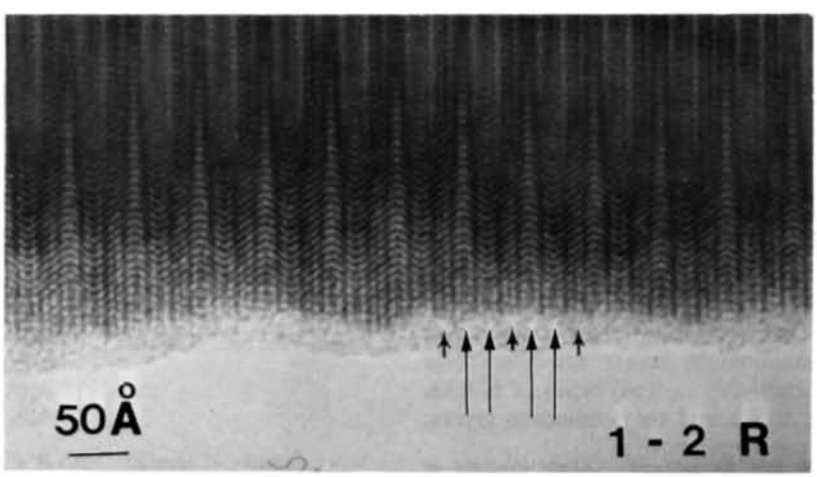

Fig. 1. Electron micrograph of the 1-2 *R* structure. $[010]_h$ incidence. The *c* axis is horizontal. Small and large arrows indicate the five and six-layer blocks.

large arrows. This region should be the 2-1 *H* structure. An irregular array of white spots at the centers of the six-layer-block units will be discussed in a later section (see Figs. 7 and 8).

Fig. 3 reproduces an electron micrograph from the 1-4 *R* structure. The five-layer blocks are indicated by arrows. In this case the *c* lattice period is 262 Å. The longest *c* lattice period so far observed is that of the 1-14 *R* structure shown in Fig. 4. Again, the five-layer blocks are marked by arrows.

(*c*) *A defect in the* 1-0 *R structure.* Fig. 5 shows an electron micrograph from a Rb_2O–Nb_2O_5 mixed crystal, in which very complex arrangements of two types of blocks are seen. The crystallite is not a single phase and various phases are locally formed as indicated in the micrograph. The thick arrows in the micrograph show the positions of defects in the 1-0 *R* structure. Single vertical white-spot arrays are present and the vertical positions of white spots in the neighboring arrays do not change from those of white spots in a single array. From this fact it is concluded that the defects are composed of three octahedron layers and are connected with the neighboring five-layer blocks in the following way; *AaBbCBbCBbCcA* . . .. Thus the hole-position sequence is *ab-b-bc* . . ., in agreement with the observation.

It should be noted here that the composition of *BbC* layers is expected from the charge balance to be

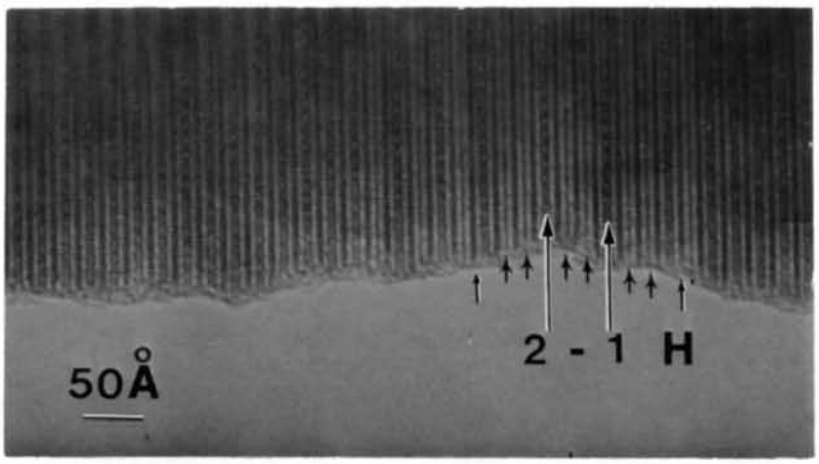

Fig. 2. An electron micrograph of a 0-1 *H* crystallite, which contains the 2-1 *H* structure. $[\bar{1}10]_h$ incidence.

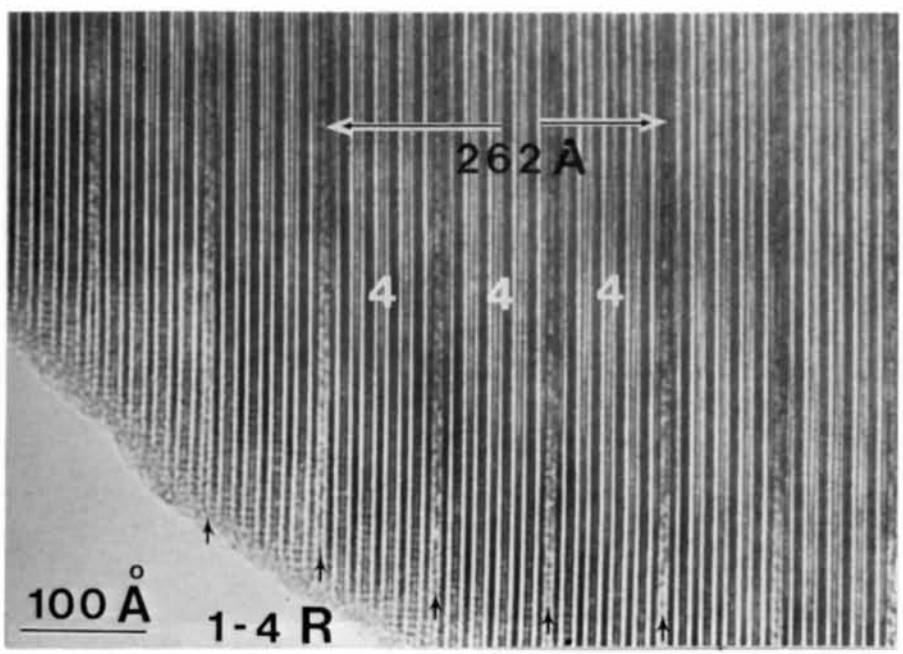

Fig. 3. 1-4 *R* structure. $[\bar{1}10]_h$ incidence.

$K_2OM_{14}O_{35}$. This means that a local deficiency of alkali ions in the 1-0 *R* structure is responsible for such a defect layer.

2.2. *Two-dimensional ordering of pentavalent ions*

(*a*) *Observations*. Fig. 6 shows an electron diffraction pattern from a 1-1 *H* crystallite with $[\bar{1}10]_h$ orientation. The *hhl* reflections with *l* odd are absent. There are diffuse streaks along $h \pm \frac{1}{3}, h \pm \frac{1}{3}, l$ lines. The very weak superstructure spots in Fig. 8(*a*) in part I should correspond to cross sections of these streaks with the Ewald sphere of $[001]_h$ incidence. The corresponding electron micrographs are shown in Fig. 7. The micrographs were taken with an objective aperture of size shown in Fig. 6. In the image two kinds of vertical white-spot array are seen. The closely spaced spot arrays indicated by thin vertical arrows are at the positions of isolated octahedron layers. The spacing, 3·8 Å, is that expected from the hexagonal unit cell. Widely spaced arrays, indicated by thick vertical arrows, whose spacing is three times that of the former,

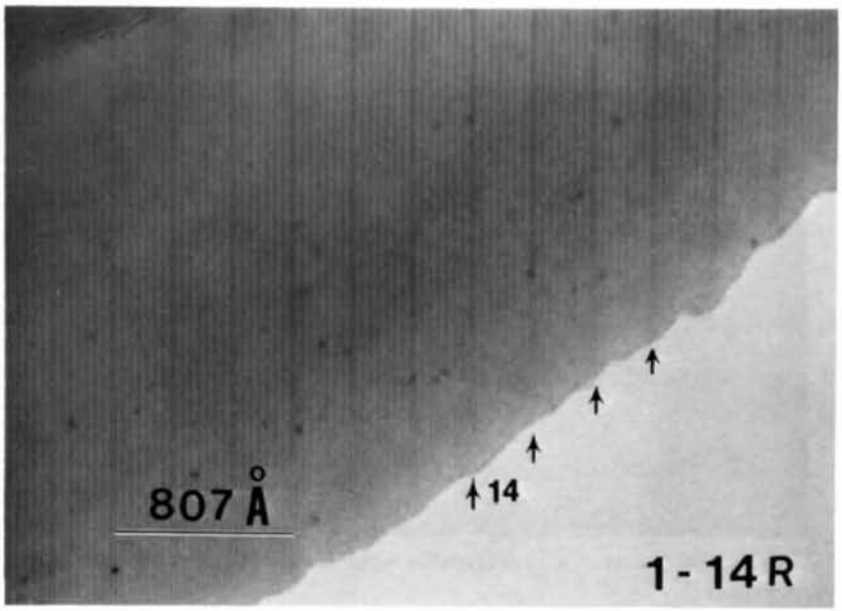

Fig. 4. 1-14 *R* structure.

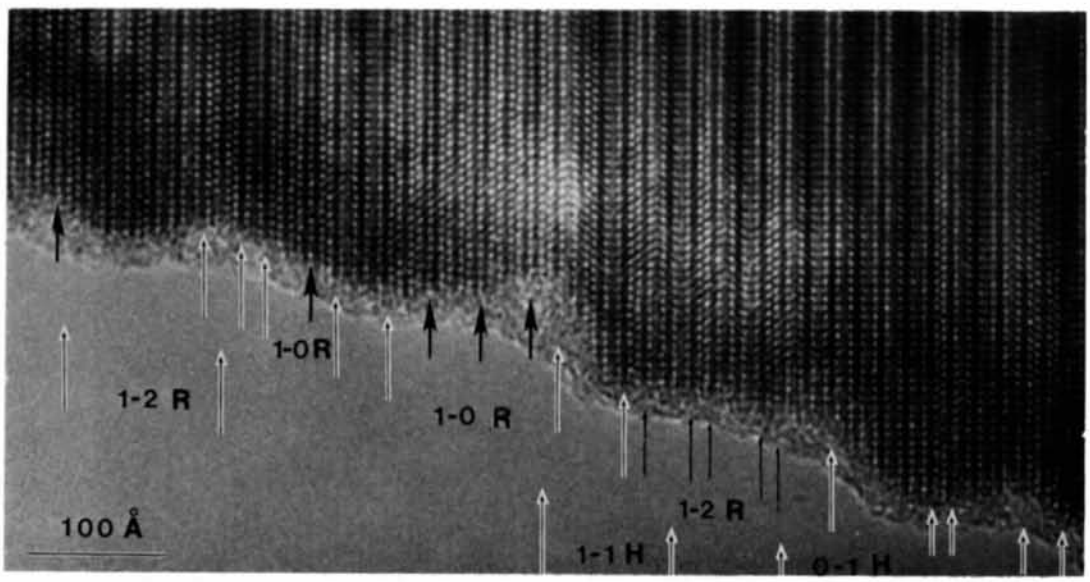

Fig. 5. An electron micrograph of a crystallite, which contains various intergrowth phases and faults (indicated by bold arrows) in the 1-0 *R* structure in the Rb_2O–Nb_2O_5 system.

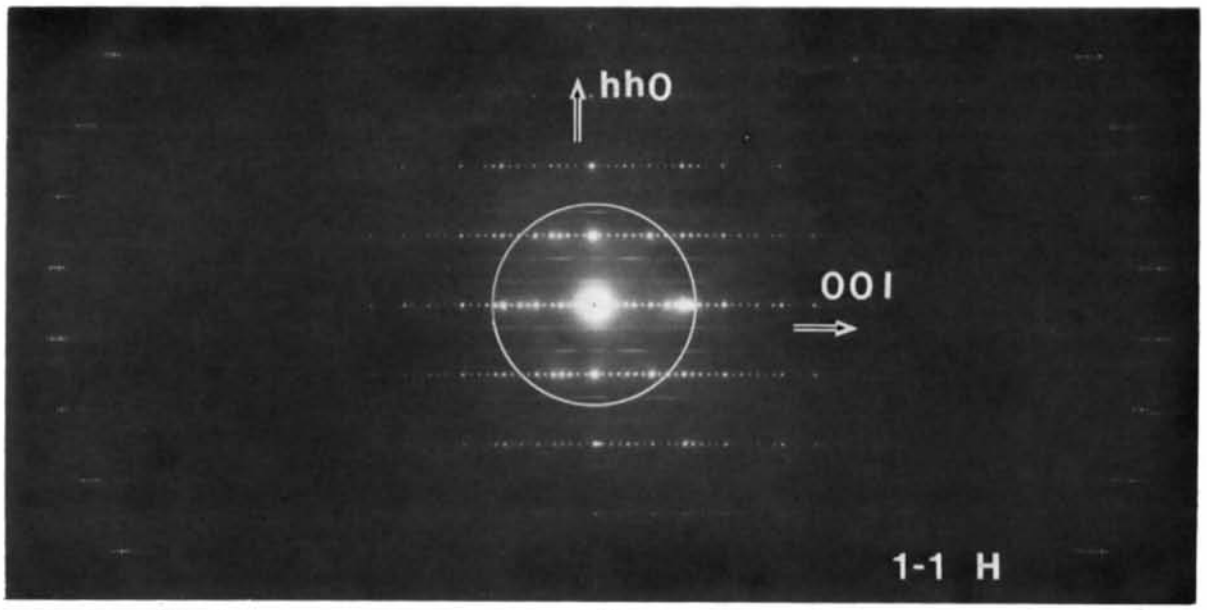

Fig. 6. An electron diffraction pattern from a 1-1 *H* crystallite with $[\bar{1}10]_h$ incidence. Diffuse streaks which have maxima and minima are along the $[00l]_h$ direction.

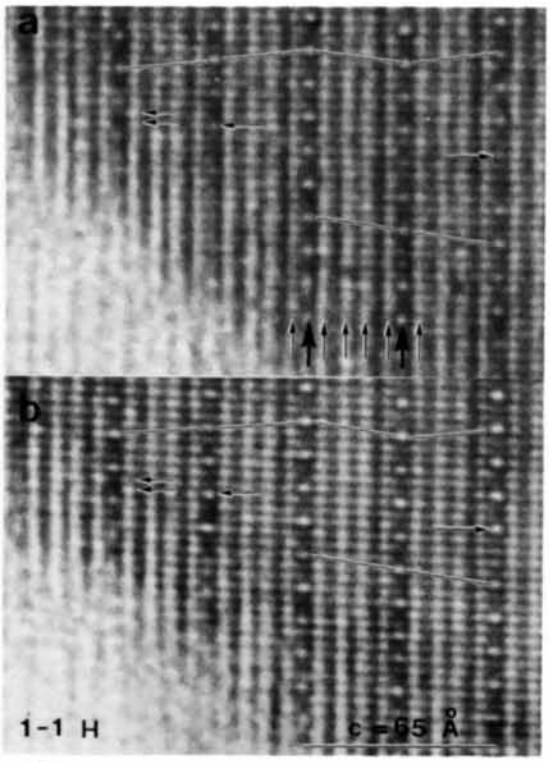

Fig. 7. Electron micrographs of a 1-1 *H* crystallite in the K_2O–Ta_2O_5 system with $[\bar{1}10]_h$ incidence (*a*) before and (*b*) after strong electron irradiation. Thin vertical arrows indicate the positions of the isolated-octahedron layer and thick solid arrows, the mirror planes of the six-layer block. The positions of white spots at the mirror planes change from place to place as shown by vertical lines. The horizontal arrows indicate the places where white-spot intensities changed from (*a*) to (*b*).

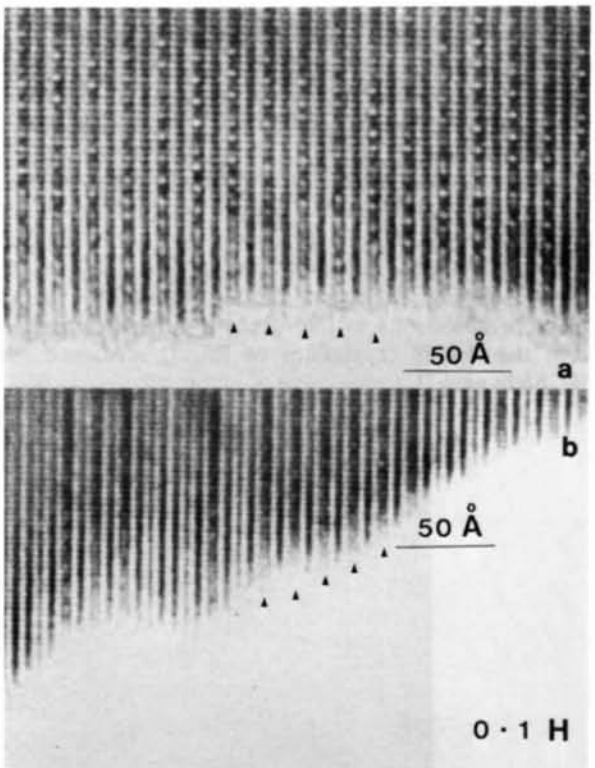

Fig. 8. Electron micrographs of a 0-1 *H* in the system K_2O-Ta_2O_5 with $[\bar{1}10]_h$ incidence. (*a*) Two-dimensionally ordered crystallite. The degree of order in one plane (represented by the vertical length of periodic white-spot array) is lower than that in Fig. 7. (*b*) Nearly disordered crystallite.

are at positions between the two successive HTB-like layers, the positions of the mirror planes in the six-layer blocks. Thus, a two-dimensional superstructure ordering in this plane is deduced. A notable fact is that the vertical positions of white spots in the widely spaced arrays change not only from array to array but also within an array and there is no regularity in their position sequence (see also Fig. 8*a*). It is evident that these widely spaced arrays give rise to the diffuse streaks in the diffraction pattern. The streaks are not continuous and have maxima, whose positions have been found to change from sample to sample and to change after strong electron irradiation. The micrograph (*b*) was taken after strong electron irradiation without a condenser aperture, which caused severe local heating. However, by comparing (*a*) and (*b*), it is seen that the positions of widely spaced spots do not change very much although there are relative intensity changes not only in the widely spaced spots but also in the closely spaced spots, as indicated by horizontal arrows. This point will be discussed later.

The kind of partial ordering was clearly seen in the 1-1 *H* crystallites of the K_2O–Ta_2O_5 mixed oxide. However, the degree of order was relatively weak for the 0-1 *H* structure. It also changed from sample to sample. Fig. 8 shows electron micrographs of 0-1 *H* crystallites which show relatively high and low degrees of ordering at mirror planes. It is seen that in (*a*) the white spots at the mirror planes are not regular and in (*b*) the white spots are very faint. The micrograph in Fig. 2 also shows some sort of ordering in the six-layer blocks. The corresponding diffraction pattern from a weakly ordered sample is shown in Fig. 9. Diffuse streaks are very faint and broad. This may be the reason why it was very difficult to see the superstructure reflections in the electron diffraction pattern from the 0-1 *H* crystallites of $[001]_h$ incidence (see Fig. 6*b* in part I).

(*b*) *Structure model for the ordering.* A structure model which gives rise to the white spots at the mirror plane of the six-layer block in Figs. 7 and 8 is shown in Fig. 10. The black spots indicate the positions of some kind of ion and the open circles are vacancies. The ions are in an ordered $\sqrt{3}a$ structure, where a is the unit-cell length of the original hexagonal cell. From the model it is clear that the ordering can be seen from the $[1\bar{1}0]_h$ (or $[110]_h$) direction and the positions of open arrows correspond to the white spots in the micrograph. The image seen from the $[110]_h$ (or $[010]_h$) direction is insensitive to the ordering. The ordering ions must be alkali ions or pentavalent ions. However, the latter are more probable for the following reasons: (1) The white-spot arrangement at the mirror planes does not change drastically after strong electron irradiation (Fig. 7*a*, *b*), probably because pentavalent ions at the mirror plane

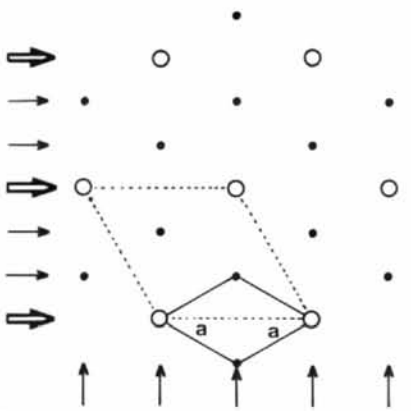

Fig. 10. The ordered arrangement at the mirror plane of the six-layer block. The original hexagonal unit cell is shown by solid lines. Dotted lines show the $\sqrt{3}a$ structure. The ordered state can be seen from the $[110]_h$ direction but not from $[1\bar{1}0]_h$ direction. Open arrows indicate the positions where vacancy sites (open circles) are seen to be white.

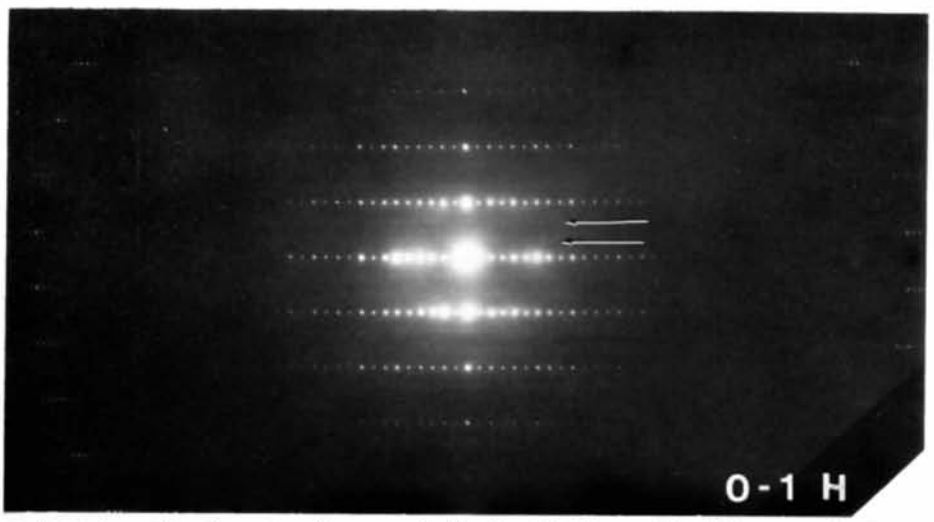

Fig. 9. An electron diffraction pattern from a nearly disordered 0-1 *H* crystallite. Diffuse scattering is very weak.

are less mobile than alkali ions. (2) As discussed in part I, the 1-0 *R* structure should have a lower mol% of alkali-metal oxides than the 0-1 *H* structure if all the pentavalent ions were in the form of MO_6 octahedra (see Appendix *A*). To decrease the mole fraction of alkali oxide for the 0-1 *H* structure, additional pentavalent ions must be located at the positions of densely packed octahedra, *i.e.* at the mirror planes of the six-layer block. Such an arrangement can be said to be favorable from the point of view of local charge balance.

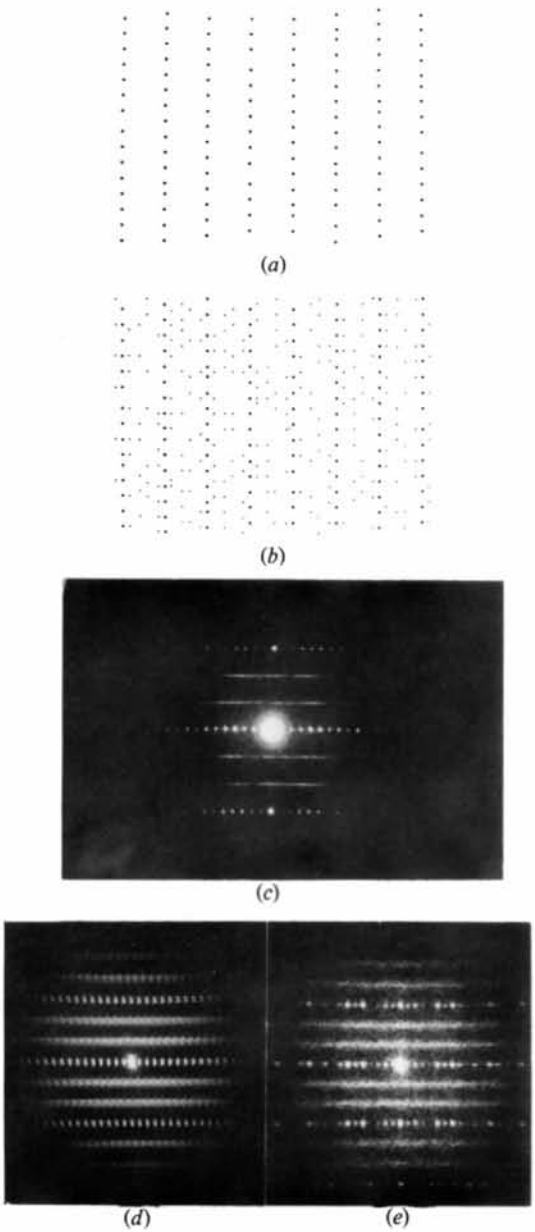

Fig. 11. Pinhole models (*a*) and (*b*) used to explain the origin of diffuse scattering in Fig. 6. (*a*) A model, where only the ordering at the mirror plane is responsible for diffuse scattering. (*b*) A model, where arrangements of alkali ions in the isolated octahedron layers as well as ordering at the mirror plane are responsible for the diffuse scattering. Optical diffraction patterns (*c*), (*d*) and (*e*). (*c*) from electron micrograph in Fig. 7(*a*), (*d*) and (*e*) from pinhole arrangement in (*a*) and (*b*) respectively. In (*c*) and (*e*) diffuse maxima are seen.

From the images in Fig. 7 the two-dimensional ordering of the pentavalent ions at the mirror plane has no relation with the type of ordering in the neighboring mirror planes. If, however, the diffuse scattering were due simply to the ordering at the mirror planes, it should have been continuous. The fact that there are many intensity maxima indicates that these maxima are caused by the special correlation between the white spots at the mirror plane and the other white spots at the isolated-octahedron layers, *i.e.* by the correlation of ordering between the ordered pentavalent ions at the mirror planes and alkali-metal ions which should be located at the isolated-octahedron layers and the hexagonal holes in the HTB-layers. This may be the reason why the positions of diffuse maxima change after strong electron irradiation, though strong irradiation does not cause drastic change in the ordering at the mirror plane, as seen in Fig. 7.

In order to confirm whether the diffuse maxima are due to the correlation mentioned above, the optical diffraction patterns were taken from the image in Fig. 7 and from the pinhole arrangements in Fig. 11(*a*) and (*b*). They are shown in Fig. 11(*c*), (*d*) and (*e*) respectively. In model (*a*), only the correlation of the pentavalent ions in the mirror planes is taken into account. The corresponding diffraction pattern in (*d*) shows no diffuse maxima. In model (*b*), the correlation between the pentavalent ions and alkali metal ions is taken into account and the corresponding pattern in (*e*) shows some diffuse maxima, as seen in (*c*).

2.3. *Comparison of observed and calculated images*

The image of the 1-1 *H* structure was calculated based upon the model shown in Table 3 proposed in the present study. The parameters in Table 3 are derived in the way shown in Appendix *B*. The program system developed for two-dimensional image calculation by Skarnulis, Iijima & Cowley (1976) and modified by M. A. O'Keefe was used. The electron-optical parameters used for calculation are given in Table 4. The results for $[010]_h$ incidence are shown in Fig. 12, where the *c* axis

Table 3. *The structure model for* 1-1 *H of* K_2O–Ta_2O_5

Chemical formula	$K_{9\cdot27}Ta_{25\cdot67}O_{69}$ (26·5 mol% K_2O)
Lattice parameters	$a = 7\cdot520$, $c = 65\cdot12$ Å
Height of HTB-like layer	3·838 Å
Height of isolated-octahedron layer	2·303
Separation between the double HTB-like layer	2·081

is horizontal. The 900 Å underfocus image reproduces the observed image of the 1-1 *H* structure shown in Fig. 7 of part I with the white-spot sequence *a-ab-bb-ba-a*.

The calculation for $[\bar{1}10]_h$ incidence for the ordered 1-1 *H* structure could not be made, since the number of atoms in the unit cell and the number of beams necessary for the image calculation were too large for the program then available. To reduce these numbers, the calculation was performed assuming a hypothetical six-layer-block structure with and without pentavalent ions at the mirror plane. The results are shown in Fig. 13, (*a*) with and (*b*) without ions, where the vertical arrows indicate the positions of mirror planes. Neighboring white spots correspond to the positions of isolated-octahedron layers. It is seen that white spots in the case without pentavalent ions at the mirror plane are brighter than those in the case with ions, in agreement with the observation. However, the positions of these spots are out of phase from those in the isolated octahedron layers, in contradiction to the observed images in Fig. 7.

Table 4. *Electron-optical parameters*

Accelerating voltage		100 kV
Spherical abberation constant		1·8 mm
Depth of focus		125 Å
Aperture size		0·35 Å^{-1}
Number of beams	$[010]_h$ incidence	489
	assumed ($[\bar{1}10]_h$)	305

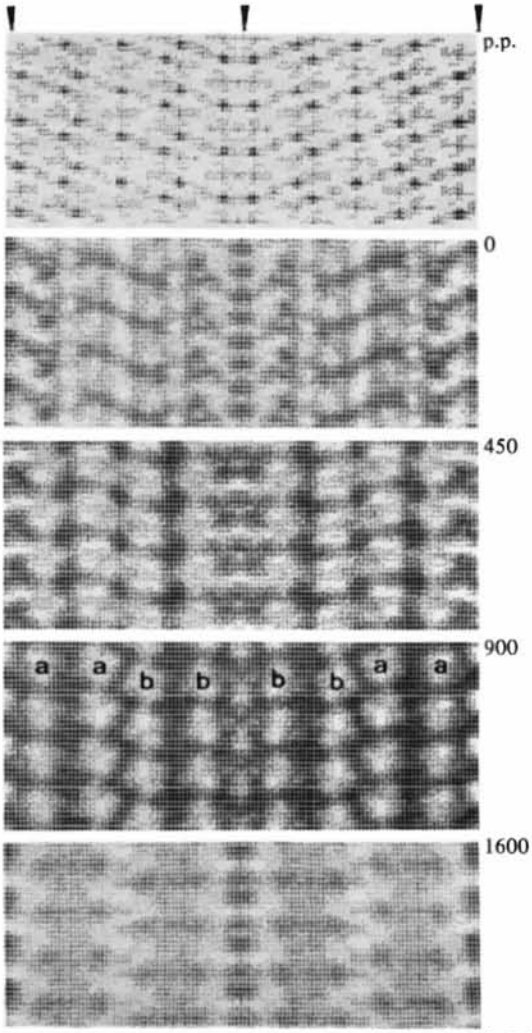

Fig. 12. $[010]_h$ projected potential (p.p.) of disordered 1-1 *H* structure (K_2O–Ta_2O_5) and calculated images for 0, 450, 900 and 1600 Å underfocus. The horizontal direction is parallel to the *c* axis. The mirror plane in the six-layer block is indicated by arrows. The optimum defocus (900 Å underfocus) image reproduces the observed one.

3. Summary and discussion

Various intergrowth phases are found which can be conveniently denoted by *n-m H* or *n-m R* depending on the odd or even number of *m*, where *n* and *m* are successive numbers of the five and six-layer blocks in the intergrowth phase structures. All the structures are characterized by the sequence rules for the two types of block given in Table 1. These rules are a natural consequence of the characteristics of the pyrochlore structure.

The calculated image for the 1-1 *H* structure agrees with that observed. Thus, the structures proposed in the

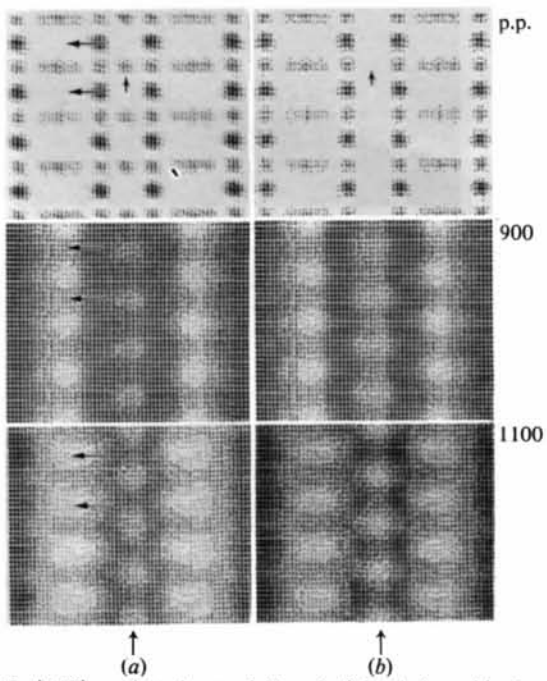

Fig. 13. $[110]_h$ projected potential (p.p.) of the six-layer block unit and its calculated image (*a*) with and (*b*) without pentavalent ions (small arrows) at the mirror plane (thick arrows). The mirror plane is brighter in (*b*).

present study based upon the white-spot arrangement when viewed along the $[010]_h$ direction are plausible, although the fine details and positions of alkali ions should be determined by the X-ray study.

Two-dimensional superstructure ordering of pentavalent ions at the mirror plane of the six-layer block was observed. Such an arrangement is favorable for local charge balance. This explains the fact that the 0-1 *H* phase contains fewer alkali ions than the 1-0 *R* phase. There is not correlation between the method of ordering in the neighboring six-layer blocks in the 0-1 *H* structure or in the 1-1 *H* structure. In the former case, the ordered area is smaller than in the latter case (compare Fig. 7 with Fig. 8). The image calculation for the ordered state could not be made. The calculated image for a hypothetical structure with and without pentavalent ions at the mirror plane, however, did not reproduce very well that observed. The reasons for the discrepancy may be: (1) The $[110]_h$ lattice spacing is about 3·7 Å and is close to the resolution limit of the microscope.* (2) The hypothetical model does not represent the actual ordered state. (3) The white spots in Figs. 7 and 8 are seen clearly only in thick areas. Further higher-resolution study may be necessary.

The characteristics of the series of structures found in the present study may be summarized as follows: (1) All structures are closely related to the pyrochlore structure. (2) The pyrochlore structure is modified so as to satisfy the local charge neutrality and to reduce the accommodation number of the alkali ions by forming double HTB-like layers (1-0 *R* structure), defect layers in 1-0 *R* structure and the six-layer blocks.

One of the present authors (KY) expresses his sincere thank to Professor J. M. Cowley for providing him the opportunity to stay at ASU and for his continuous encouragement and advice. Thanks are also due to Dr S. Iijima for much technical advice and discussion concerning high-resolution electron microscopy. Thanks are also to Drs A. J. Skarnulis and M. A. O'Keefe for their programs for the image calculation. This work was partially supported by the Ministry of Education of Japan and by USA National Science Foundation grants GH 36668 and DMR 76-06108.

APPENDIX *A*

The five-layer block is composed of *AaBbC* octahedron layers. In the unit cell a HTB-like layer (*A*, *B* or *C*) has three octahedra and an isolated-octahedron layer has one octahedron. Thus, 11 octahedra are in the five-layer block. Since *A* and *C* layers form double HTB-like layers together with the neighboring blocks, 30 oxygen ions are said to belong to 11 octahedra: 6 pentavalent ions in *A* and *C* layers share 15 oxygen ions and 5 pentavalent ions in *aBc* layers share 15 oxygen ions. Thus, the oxygen pentavalent ion ratio in the five-layer block is $30/11 = 2{\cdot}73$. Similar consideration for the six-layer block like *AaBB'a'A'* shows that this ratio is $(15 + 24)/14 = 2{\cdot}79$, which is slightly larger than that for the five-layer block. This indicates that the molar fraction of alkali oxide for the 0-1 *H* structure (9*L*) should be larger than for the 1-0 *R* structure (11*L*), contrary to the experimental results (see Fig. 1 in part I). If two positions out of three in the mirror plane in the six-layer block are occupied by pentavalent ions, as shown in Fig. 10, the above ratio decreases to $39/(14 + 2/3) = 2{\cdot}66$. Note that the oxygen pentavalent ion ratios for samples which show the 1-0 *R* structure (11*L*) (Nos. 2 and 4 in Table 2 of part I) is 2·70 and that for the 0-1 *H* structure (9*L*) (Nos. 1 and 3) is 2·67 and that these values are close to 2·73 and 2·66 calculated above.

APPENDIX *B*

First, we assumed that the HTB-like layers and isolated octahedron layers are composed of ideal octahedra and are identical with those in the pyrochlore structure. From the *a* lattice parameter the height of an octahedron was determined. From the height, the thicknesses of the six-layer block and the five-layer block were determined from simple geometrical considerations. Since the *c* lattice parameters are the sum of the thickness of the constituting blocks and the relaxation distances at the double HTB-like layers, the relaxation distance can be determined from the *c* lattice parameters of the 0-1 *H* and 1-0 *R* structures independently and was found to be consistent, as shown in Table 3. Thus, the octahedron framework in the 1-1 *H* structure was determined. The positions of the ions are assumed in the following way.

Pentavalent ion (Ta): (1) the centers of the octahedra, (2) at the mirror plane. The occupation number is 2/3.

Oxygen ions: corners of the octahedra. At the double HTB-like layer, the occupation number is 1/2. No displacement for the relaxation was taken into account.

Alkali ion (K): The number of alkali ions was derived from the numbers of pentavalent ions and oxygen ions so as to satisfy the charge balance and the observed chemical composition. Their positions are at the isolated-octahedron layers but displaced to the center of the hexagonal holes in the neighboring HTB-like layers.

References

IIJIMA, S. (1971). *J. Appl. Phys.* **42**, 5891–5893.

SKARNULIS, A. J., IIJIMA, S. & COWLEY, J. M. (1976). *Acta Cryst.* A**32**, 467.

YAGI, K. & ROTH, R. S. (1978). *Acta Cryst.* A**34**, 765–773.

* Note that the small holes at the isolated-octahedron layers indicated by horizontal arrows in the projected potential in Fig. 13 are seen as white holes in the 1100 Å underfocus image but not in the −900 Å optimum focus image.